

# Laboratory Performance Evaluation of Modified Asphalt Mixtures for Incheon Airport Pavements

HYUN-JONG LEE<sup>a\*</sup>, JO S. DANIEL<sup>b</sup> and Y. RICHARD KIM<sup>c†</sup>

<sup>a</sup>Department of Civil Engineering Kangnung National University Kangnung, Kangwondo 210-702, Korea, <sup>b</sup>Graduate Research Assistant Department of Civil Engineering North Carolina State University and <sup>c</sup>Associate Professor P.O. Box 7908 Department of Civil Engineering North Carolina State University Raleigh, NC 27695-7908

(Received January 19, 1998; In final form July 29, 1999)

In this paper, fatigue and rutting characteristics of various modified and unmodified mixtures are evaluated using uniaxial tension and triaxial compression cyclic tests, respectively. The fatigue and healing behavior of the mixes is presented by means of the viscoelastic, continuum damage (VCD) model previously developed by the authors. Since the VCD model takes the same form as the classical, strain-based fatigue model, the coefficients in the classical model are described in terms of fundamental material properties and test conditions in the VCD model. The explicit form of the VCD model and different performance data from all the mixes are used to investigate the effects of the material properties on the fatigue life and microdamage healing potential of asphalt concrete. Structural analysis based on the multi-layered elastic theory is conducted to compare the fatigue lives of the various mixes in pavement systems.

A simple permanent deformation model that correlates vertical permanent strain and number of applied loads is used in representing the data from the triaxial compression tests at different confining pressures. The modified mixtures demonstrate better rutting resistance as expected, although the ranking among the modified mixtures changes depending on the confining pressure. The role of additive at high temperatures and different gradations and binder contents used in the modified mixtures seem to explain these observations.

*Keywords:* Modified Asphalt Mixtures, Fatigue, Healing, Rutting, Viscoelasticity, Damage

## INTRODUCTION

The Korean Airport Construction Authority plans to build an international airport at YongJong-Do, Korea. Pavements in the airport are designed based on the FAA airport pavement thickness design method even

though the materials and environmental conditions of Yong Jong-Do pavements are different from those used in developing the FAA design equations. Daebon Engineering Corp. (DEC) was charged to build and evaluate test pavement sections to verify the thickness designs and has developed a comprehensive

\* Phone: 82-391-640-2419 FAX: 82-391-640-2244 E-mail: hlee@knusun.kangnung.ac.kr

† Phone: 919-515-7758 FAX: 919-515-7908 E-mail: kim@eos.ncsu.edu

plan to instrument these pavements with sensors to measure pavement responses (stresses, strains, and deformations) under simulated loading conditions.

As a part of this work, laboratory fatigue and permanent deformation models were applied to the various modified and unmodified mixtures used in the field test pavement project. The principal objectives of the work conducted at North Carolina State University were: (1) to determine the viscoelastic material properties of the asphalt mixtures at varying loading frequencies; and (2) to evaluate the fatigue and rutting performance of the different asphalt mixtures. Eventually, the laboratory prediction models were used to provide information on performance ranking of these mixtures in terms of fatigue and rutting.

There are seven different asphalt mixtures used in the construction of the test sections, five mixtures for the surface course and two for the base course. The materials for the surface course include a conventional dense graded asphalt mixture, Stone Matrix Asphalt, and asphalt mixtures modified with Latex (SBR), SBS, and Gilsonite (hereafter called S19, SMA, SBR, SBS, and GIL mixtures, respectively). The two materials used for the asphalt concrete base course are a conventional asphalt base course and asphalt modified with Chemcrete (hereafter called B25 and CHE mixtures, respectively).

Uniaxial tensile creep tests were performed to measure viscoelastic material properties of each mixture. Relaxation modulus and dynamic modulus were predicted from the creep data using theory of linear viscoelasticity. Uniaxial tensile fatigue tests were conducted on the seven asphalt mixtures to evaluate fatigue performance. A mechanistic fatigue performance prediction model proposed by Lee and Kim (1998a, 1998b), and Lee *et al.* (1998) was used to estimate the fatigue lives of the mixtures. Rutting performance was evaluated for five surface course materials by performing triaxial compression tests. A typical permanent deformation model was adopted in this study to model the permanent deformation of the mixtures.

## PERFORMANCE PREDICTION MODELS

### Fatigue Prediction Models

The two main approaches in the fatigue characterization of asphalt mixtures are phenomenologically and mechanistically based approaches. One of the most commonly used phenomenological fatigue models relates the *initial* response (such as tensile strain) of an asphalt mixture to the fatigue life:

$$N_f = a(\varepsilon_0)^b \quad (1)$$

where

- $N_f$  = number of cycles to failure,
- $\varepsilon_0$  = initial strain response, and
- a, b = regression coefficients.

This phenomenological model is simple to use because only the mixture response at the initial stage of fatigue testing needs to be measured. This model does not account for how damage evolves throughout the fatigue life, and hence it is only valid for a given set of loading conditions (Dijk and Visser 1997) and may need additional means to account for complex damage under realistic loading conditions (e.g., multi-level loading, rest periods, etc.).

Recently, a uniaxial constitutive model of nonaging asphalt-aggregate mixtures has been developed by the authors (Kim *et al.* 1997, Lee and Kim 1998a, 1998b). It employs the elastic-viscoelastic correspondence principle (Schapery 1984) and Schapery's work potential theory (Schapery 1990) to model the mechanical behavior of asphalt concrete under cyclic loading with rest periods. It was proven by the laboratory experimental study that this model was able to predict hysteretic stress-strain behavior of asphalt concrete under different loading histories (monotonic and cyclic), varying rates of loading, different modes-of-loading (controlled-stress and controlled-strain), various stress/strain amplitudes, and random rest periods.

Based on the constitutive model described above, Lee *et al.* (1999) developed a simplified fatigue performance prediction model as follows:

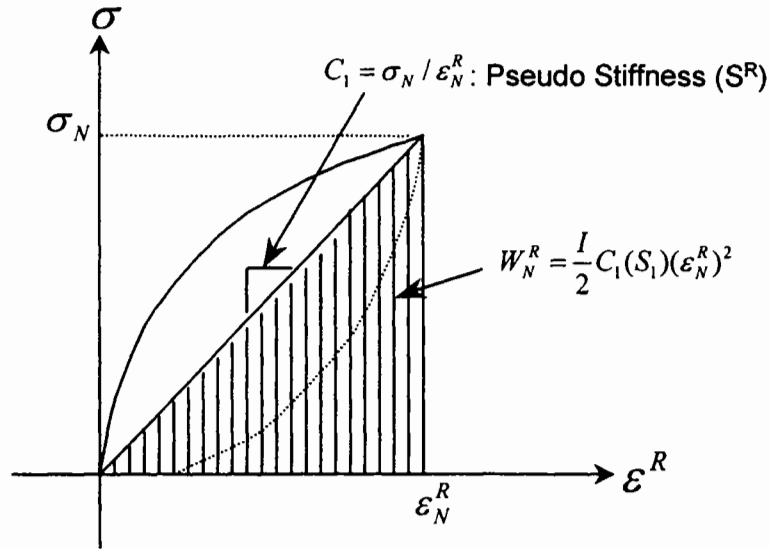


FIGURE 1 Pseudo Stiffness and Pseudo Strain Energy Density Function

$$N_{f,Total} = N_{f,w/oRP} + \sum_{i=1}^M \Delta N_{f,i} \quad (2)$$

where

$N_{f,Total}$  = number of load repetitions to failure with multiple rest periods,

$N_{f,w/oRP}$  = number of load repetitions to failure without any rest,

$N_{f,i}$  = increase in  $N_f$  due to the  $i^{\text{th}}$  rest period, and

$M$  = total number of rest periods.

To determine the explicit form of  $N_f$  equation in (2), the following damage evolution law applicable to viscoelastic media (Schapery 1990, Park et al. 1996) was used:

$$\frac{dS_m}{dN} = \left( -\frac{\partial W_N^R}{\partial S_m} \right)^{\alpha_m} \quad (3)$$

where

$S_m$  = internal state variables (ISVs) representing any structural changes in the system,

$N$  = number of applied loads,

$W_N^R$  = maximum value of pseudo strain energy density function in the  $N^{\text{th}}$  cycle,

$\alpha_m$  = material constants, and

$m = 1, 2, 3, \dots, M$ .

Equation (3) is similar in form to a crack growth law in fracture mechanics for viscoelastic materials.

For a cyclic loading condition under the controlled-strain mode, the maximum pseudo strain energy density function was proposed to be a function of the peak pseudo strain and an ISV as follows (Lee and Kim 1998b, Lee et al. 1999):

$$W_N^R = \frac{I}{2} C_1(S_1) (\varepsilon_N^R)^2 \quad (4)$$

where

$I$  = initial pseudo stiffness,

$C_1 = C_{10} + C_{11}(S_1)^{C_{12}}$  = damage function,

$$S_1 \cong \sum_{i=1}^N \left[ \frac{I}{2} (\varepsilon_{N,i}^R)^2 (S_{i-1}^R - S_i^R) \right]^{\frac{\alpha_1}{(1+\alpha_1)}} (t_i - t_{i-1})^{\frac{1}{(1+\alpha_1)}}$$

$\varepsilon_N^R$  = peak pseudo strain in the  $N^{\text{th}}$  cycle,

$$\varepsilon^R = \frac{1}{E_R} \int_0^t E(t - \tau) \frac{d\varepsilon}{d\tau} d\tau$$

= uniaxial pseudo strain (5)

Figure 1 shows a typical stress-pseudo strain curve under a cyclic load. As shown in this figure, the

pseudo stiffness, denoted by  $S^R$ , is defined as the slope of the stress-pseudo strain loop (i.e.,  $\sigma_N/\varepsilon_N^R$ ). The pseudo stiffness decreases as cyclic loading continues due to fatigue damage in the system, which is represented by the function  $C_1$ . The  $S_1$  in Equation (4) is the first ISV representing the fatigue damage growth in the system.

The  $N_f$  equation without rest periods may be obtained by integrating Equation (3) after the substituting in Equations (4) and (5):

$$N_{f,w/oRP} = A\varepsilon_0^{-2\alpha_1} \quad (6)$$

where

$$A = \frac{f(S_{1f})^{p_1}}{p_1(0.125IC_{11}C_{12})^{\alpha_1}} |E^*|^{-2\alpha_1}$$

$$\alpha_1 = 1 + 1/n,$$

$n$  = slope of the creep compliance versus time curve in log-log scales,

$$p_1 = 1 + (1 - C_{12})\alpha_1,$$

$C_{11}$ ,  $C_{12}$  = damage coefficients to be determined from experiments,

$S_{1f}$  = the value of damage parameter at failure,

$\varepsilon_0$  = tensile strain amplitude,

$f$  = loading frequency, and

$|E^*|$  = dynamic modulus.

The  $N_{f,w/oRP}$  is a function of damage evolution characteristics of the material ( $C_{11}$  and  $C_{12}$ ), viscoelastic material properties ( $n$  and  $|E^*|$ ), fatigue test conditions ( $\varepsilon_0$  and  $f$ ), and a failure criterion ( $S_{1f}$ ).

The major difference between the fatigue model in Equation (6) and the phenomenological fatigue model in Equation (1) is that all the coefficients in the fatigue model in Equation (6) are represented by engineering parameters except the coefficients  $C_{11}$  and  $C_{12}$ . These regression coefficients are necessary to model the nonlinear behavior of the material as it is undergoing damage. Pavement engineers may be able to use the fatigue model in Equation (6) as a tool to select or design more fatigue resistant asphalt mixtures by investigating ways of changing the param-

eters in ways that improve the fatigue life of the mixture.

Similarly, Lee *et al.* (1999) proposed the following equation for determining the increase in fatigue life due to a rest period:

$$\Delta N_{f,i} = \frac{f(S_{3e})^{p_3}}{p_3[0.125I(C_2 + S_B^R)C_{31}C_{32}]^{\alpha_3}} |E^*|^{-2\alpha_3} (\varepsilon_0)^{-2\alpha_3} \quad (7)$$

where

$$p_3 = 1 + (1 - C_{32})\alpha_3,$$

$C_2 = C_{20} + C_{21}(S_2)^{C_{22}}$  = increase in pseudo stiffness during the rest period,

$C_{31}$ ,  $C_{32}$  = damage coefficients after rest periods to be obtained from experiments,

$$S_2 \cong \left[ \frac{I}{2} (\varepsilon_N^R)^2 (S_A^R - S_B^R) \right]^{\frac{\alpha_2}{1+\alpha_2}} t_{RP}^{\frac{1}{1+\alpha_2}},$$

$\alpha_2$ ,  $\alpha_3$  = material constants to be obtained from experiments,

$$S_3 = \int_0^1 \left[ -\frac{IS_A^R}{2} \frac{d(S^R/S_A^R)}{dt} (\varepsilon_N^R)^2 \right]^{\frac{\alpha_1}{1+\alpha_3}} dt,$$

$S_{3e}$  = a value of damage parameter  $S_3$  when  $S^R = S_B^R$ ,

$S_B^R$  = pseudo stiffness immediately before the rest period, and

$S_A^R$  = pseudo stiffness immediately after the rest period.

Detailed steps involved in the development of the fatigue models in Equations (6) and (7) can be found in Lee *et al.* (1999). Substituting Equations (6) and (7) into Equation (2) gives the final equation:

$$N_{f,Total} = \frac{f(S_{1f})^{p_1}}{p_1(0.125IC_{11}C_{12})^{\alpha_1}} |E^*|^{-2\alpha_1} \varepsilon_0^{-2\alpha_1} + \sum_{i=1}^M \frac{f(S_{3e})^{p_3}}{p_3[0.125I(C_2 + S_B^R)C_{31}C_{32}]^{\alpha_3}} |E^*|^{-2\alpha_3} \varepsilon_0^{-2\alpha_3} \quad (8)$$

In this study, both phenomenological and viscoelastic continuum damage models are applied to the fatigue characterization of asphalt mixtures.

### Permanent Deformation Model

In the last two decades, permanent deformation (rutting) has been one of the major traffic associated failure modes in asphalt concrete pavements. Especially with increases in axle load, load repetition, tire pressure, and asphalt concrete thickness, a methodology to predict permanent deformation and mitigate potential safety problems associated with this distress is needed (Sousa et al. 1990).

The layer-strain predictive methodology and viscoelastic procedure have commonly been used to predict the amount of rutting in a multi-layered asphalt pavement system (Sousa et al. 1990). The layer-strain method consists of predicting rut depths using permanent deformation characteristics determined from laboratory tests together with an analysis procedure for the pavement structure using either linear or nonlinear elastic theory. The general principle of this method was first proposed by Barksdale (1972) and Romain (1972). One of the major advantages of the viscoelastic approach is that moving wheel loads can be considered in conjunction with time-dependent material properties to define the state of stress and strain at particular points in the pavement structure. Material properties can be defined either in terms of models consisting of finite numbers of Maxwell and/or Kelvin elements in various arrangements. Detailed information on the layer-strain and viscoelastic methods is well reviewed by Sousa et al. (1990).

Since rutting in typical asphalt pavements has been found to primarily be a result of the permanent deformation in the asphalt layer (Sousa et al. 1990), this study focuses on the permanent deformation that occurs in the asphalt surface course only.

There are numerous types of permanent deformation models of asphalt concrete available. One of the most common permanent deformation models to correlate the plastic strain with number of cycles is as follows:

$$\log \varepsilon_p = k_1 + k_2 \log(N) \quad (9)$$

where

- $\varepsilon_p$  = permanent strain,
- $N$  = number of applied loads, and
- $k_1, k_2$  = regression constants.

The permanent deformation is composed of two different mechanisms: densification (volume change) and repetitive shear deformation (plastic flow with no volume changes). In general, the densification occurs at the early stage of cyclic loading while the shear deformation (plastic flow) is a long-term process. Thus, the coefficient  $k_1$  may represent the densification of the specimen. The slope of the plastic strain-number of cycle curve  $k_2$  may be more related to the characteristics of plastic flow. The coefficients  $k_1$  and  $k_2$  depend mainly on the material types and state of stress, and can be determined from the laboratory tests.

Stress states in a pavement section under the traffic loading vary from location to location. Brown and Bell (1977) proposed the use of stress invariants as the most appropriate method of representing the correct stress state for material characterization. The use of stress invariants is particularly advantageous in the tension zone at the bottom of asphalt layers and also in predicting rutting away from the axis of symmetry of loading. Wijeratne and Sergious (1987) successfully used two stress invariants, mean normal stress ( $p$ ) and shear stress ( $q$ ), to characterize the model coefficients  $k_1$  and  $k_2$  in Equation (9).

Celard (1977) emphasized, based on the dynamic creep tests, the important effect of shear stress on the rate of permanent deformation. For example, in Celard's tests, increasing the shear stress from 0.1 to 0.25 MPa increased the rate of permanent deformation from 0.1 to 10. On the other hand, varying the normal stress from 0.1 to 0.25 MPa did not significantly change the rate of permanent deformation. Similar conclusions can be derived from the work of Brown and Bell (1977).

## MATERIALS AND TESTING PROGRAM

### Materials

The asphalt cement used in this study was penetration grade 60–70 and the optimum binder content was determined by DEC using Marshall mix design

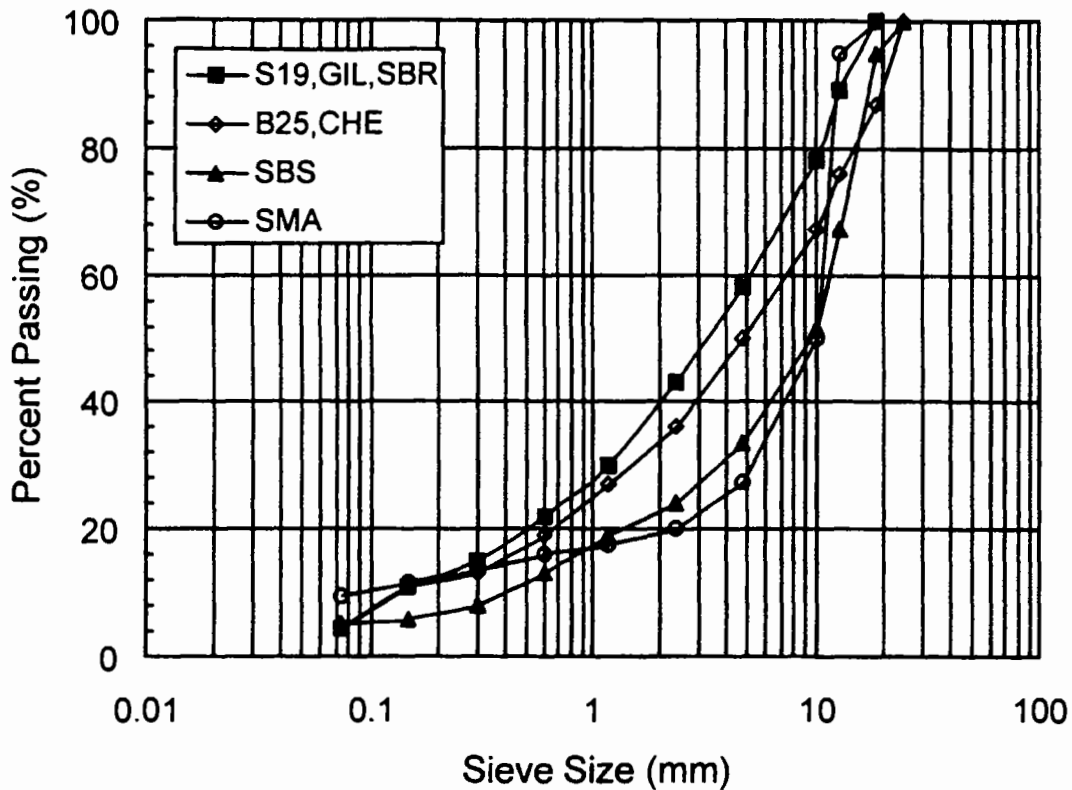


FIGURE 2 Aggregate Gradations

method. Four different types of aggregate gradations were used in this study as shown in Figure 2. As can be seen in this figure, the S19, SBR, and GIL mixtures have a typical dense gradation with nominal maximum size of aggregate (NMSA) of 19 mm. The

SMA mixture has a 12.5 mm NMSA gradation and the SBS mixture a different 19 mm gradation. For the asphalt treated base courses, B25 and CHE mixtures have the same gradation with a 25 mm NMSA.

TABLE I Mixture Information

| Mixture Type | Asphalt Content <sup>a</sup><br>(%) | Modifier Content <sup>b</sup><br>(%) | Aggregate Temp.<br>(°C) | Asphalt Temp.<br>(°C) | Mixing Temp.<br>(°C) | Compact. Temp.<br>(°C) |
|--------------|-------------------------------------|--------------------------------------|-------------------------|-----------------------|----------------------|------------------------|
| S19          | 5.8                                 | —                                    | 160                     | 150                   | 150                  | 150                    |
| SBR          | 5.5                                 | 0.440                                | 180                     | 160                   | 170                  | 160                    |
| GIL          | 5.6                                 | 0.672                                | 180                     | 160                   | 170                  | 170                    |
| SBS          | 5.3                                 | Premixed                             | 180                     | 160                   | 180                  | 160                    |
| SMA          | 6.7                                 | 0.482                                | 180                     | 150                   | 160                  | 150                    |
| B25          | 4.9                                 | —                                    | 160                     | 150                   | 150                  | 150                    |
| CHE          | 4.4                                 | 0.098                                | 180                     | 150                   | 150                  | 150                    |

a. Optimum asphalt content is by weight of dry aggregate.

b. Modifier content is by weight of dry aggregate.

The general information on component materials, mixing and compaction temperatures, and mixing procedures was provided by DEC and summarized in Table I. Two different types of cylindrical specimens, 100 mm diameter by 150 mm tall specimens for fatigue testing and 150 mm diameter by 150 mm tall specimens for rut testing, were fabricated by using a gyratory compactor. Superpave Level 1 Mix Design (1995) was used to determine the appropriate compaction parameters. Trial specimens for each mixture were compacted to determine the effort required to obtain the desired air void content of  $4 \pm 0.5\%$ . Once this was done, the test specimens were fabricated with the correct air voids.

## Testing Program

### *Uniaxial Tension Test*

All tests were conducted at 25°C in a uniaxial tension mode using a servo-hydraulic closed-loop testing machine. Creep tests were performed for the characterization of viscoelastic material properties. Load levels used in the creep tests were between 267 N and 400 N. Displacements were measured between the top and bottom loading plates, which resulted in a 150 mm gage length. Stresses and strains used in the analysis were nominal (average) values.

A haversine wave with 0.2-second loading time was used in fatigue tests. Two loading histories in the fatigue tests were used for different purposes. These loading histories were:

- 1) Constant strain amplitude cyclic loading histories without rest periods to characterize the fatigue performance of the materials, and
- 2) Constant strain amplitude cyclic loading histories with rest periods to characterize microdamage healing of the materials.

The first loading history was used to model the damage growth in asphalt concrete. In order to characterize the short, intermediate, and long term fatigue damage of asphalt concrete, four different strain amplitudes were experimentally determined to produce failure at approximately 3,000, 10,000, 50,000, and 300,000 cycles.

The second loading history was designed to evaluate and model the microdamage healing that occurs during rest periods. Three different strain amplitudes were used in these tests. Five different rest durations (20, 40, 80, 320, and 1280 seconds) were introduced between repetitive loading groups. The number of cycles in a loading group between two rest periods was large enough to eliminate the effects of the previous rest period on the current one, and to create some additional damage in the specimen. With these issues in mind, two sequences of loading and rest periods were carefully designed. The first sequence was composed of five loading blocks separated by five rest periods in increasing duration. In the second sequence, the order of the rest periods was reversed (i.e., decreasing duration). Upon completion of the second sequence, the specimens were subject to continuous cyclic loading until failure occurred.

### *Triaxial Test*

The five surface course materials evaluated in this portion of the study included S19, SBR, GIL, SMA, and SBS. Recognizing the fact that fairly thick surface courses are to be used in the Incheon airport pavement and based on published report (Sousa et al. 1990), it was decided that the evaluation of the surface materials was sufficient.

To characterize the rutting performance of the materials, triaxial tests were conducted at 60°C under different stress states using a servo-controlled pneumatic machine in the "Texas" triaxial mode. This machine has an actuator loading capacity of 5 kN on the vertical axis, and a confining pressure capacity of 400 kPa. The triaxial test method employed in this study applies the confining pressure to the perimeter of the cylindrical specimen without applying the same stress to the ends of the specimen, by exposing the ends out of the triaxial cell. Therefore, it is not necessary to start from a state of stress that is virtually hydrostatic, nor is it necessary to make corrections for loading shaft and platen areas in the computation of stress. Also, the radial pressure applied to the specimen is controlled separately from that provided by the axial actuator. Two LVDTs were used for the measurements of vertical deformations. In addition, two radial deformations were measured. An environmen-

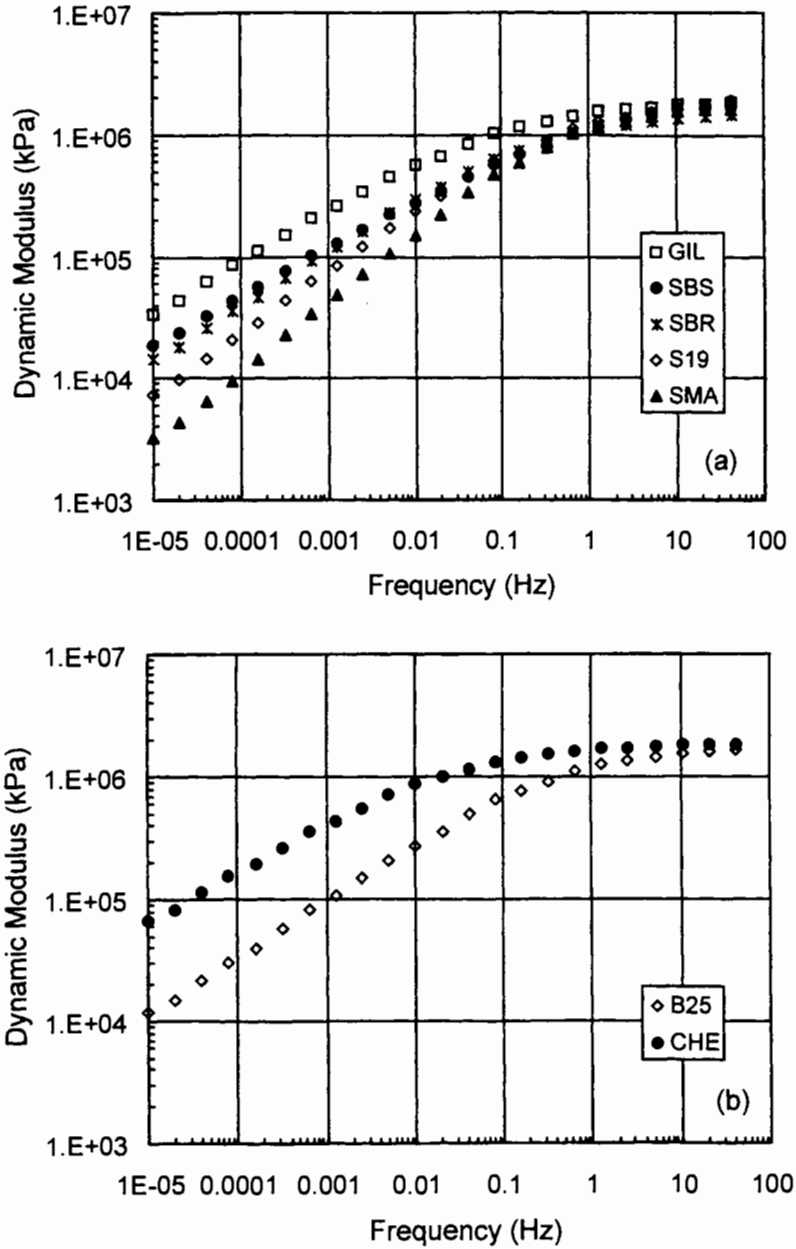


FIGURE 3 Dynamic Modulus versus Frequency: (a) Surface Mixes; (b) Base Mixes

tal chamber that accommodates the triaxial testing machine was used to maintain the test temperature.

The objective of the triaxial testing was to develop an accelerated test method by which the relative performances of the five mixtures could be determined. By definition, an accelerated test can not simulate the

conditions that occur in the field. Therefore, the loading and environmental conditions for this testing were chosen to achieve a reasonable number of cycles to failure while providing a clear distinction in rutting performance among the five mixtures.

TABLE II Stress States Used in Triaxial Compression Tests

| Identification | Stress Amplitude of Axial Loading (kPa) | Confining Pressure (kPa) | Max. Mean Normal Stress, $p$ (kPa) | Max. Shear Stress, $q$ (kPa) |
|----------------|---|--------------------------|------------------------------------|------------------------------|
| CC1            | 275                                     | 405                      | 118                                | 235                          |
| CC2            | 275                                     | 20                       | 105                                | 255                          |
| CC3            | 275                                     | 10                       | 98                                 | 265                          |

A haversine loading with 0.5 s of loading time and 1.5 s of rest period was used in the axial direction. The 0.5 s of loading time was selected because it approximately corresponds to 15 km/hr (Kim 1994), which simulates a slowly moving aircraft on the taxiway (which is a more critical condition for rutting). The 1.5 s of rest period was selected to give the specimen enough time to recover more than 95% of recoverable deformation.

Static confining pressures instead of dynamic confining pressures were used in the tests due to the constraint of the triaxial testing machine. The static confining pressures included 10, 20, and 40 kPa and the resulting stress states are summarized in Table II. The reader is reminded that shear stress  $q$  is identical to the deviator stress in the triaxial loading condition. The  $p$  and  $q$  values in Table II reduced ( $p$ ) and increased ( $q$ ) from those that would have been experienced in a test in which the confining stress was cycled about its mean value. Such modified values may be more representative for comparison with other studies (Wijeratne and Sargious 1987).

## CHARACTERIZATION OF FATIGUE PERFORMANCE

### Viscoelastic Material Properties

Creep compliance, relaxation modulus, and dynamic modulus are essential material properties in viscoelastic analysis. These viscoelastic material properties can be measured directly from laboratory tests, or can be obtained from the creep compliance through application of theory of linear viscoelasticity. In this study, only creep tests were conducted and the relaxation and dynamic moduli values of each specimen were

predicted from the creep data based on the procedure proposed by Kim et al. (1997).

Figures 3(a) and 3(b) show the typical behaviors of dynamic moduli for surface and base materials, respectively. As shown in Figure 3(a), GIL has the highest and SMA has the lowest modulus values at low frequencies (equivalent to a slow loading rate or high temperature). In the high frequency range (equivalent to a fast loading rate or low temperature), GIL has the highest modulus values while SBR has the lowest modulus values. For the base course materials, CHE has higher dynamic modulus values than B25 as shown in Figure 3(b).

### Structural Analysis of the Pavement Sections

To accurately and fairly evaluate the fatigue performances of different mixtures, it is essential to perform a structural analysis of the asphalt pavements to be constructed in the field because each mixture has a different stiffness value that results in a different structural response. There are three different pavement sections (shown in Figure 4) considered in the structural analysis. As can be seen in Figure 4(a), Section 1 is the same as Section 2 except CHE was used in the asphalt concrete base layer in Section 2 instead of conventional asphalt concrete (i.e., B25). These two pavement sections were used to evaluate the fatigue performance of the B25 and CHE mixtures. Figure 4(b) shows Section 3 that was built in the test track to evaluate the performance of the five different surface course materials.

Structural analysis was performed using the loading configuration for a special vehicle developed to apply the design loading to the test pavements in this project. The loading configuration consists of dual wheels that each carry a load of 206 kN with a tire

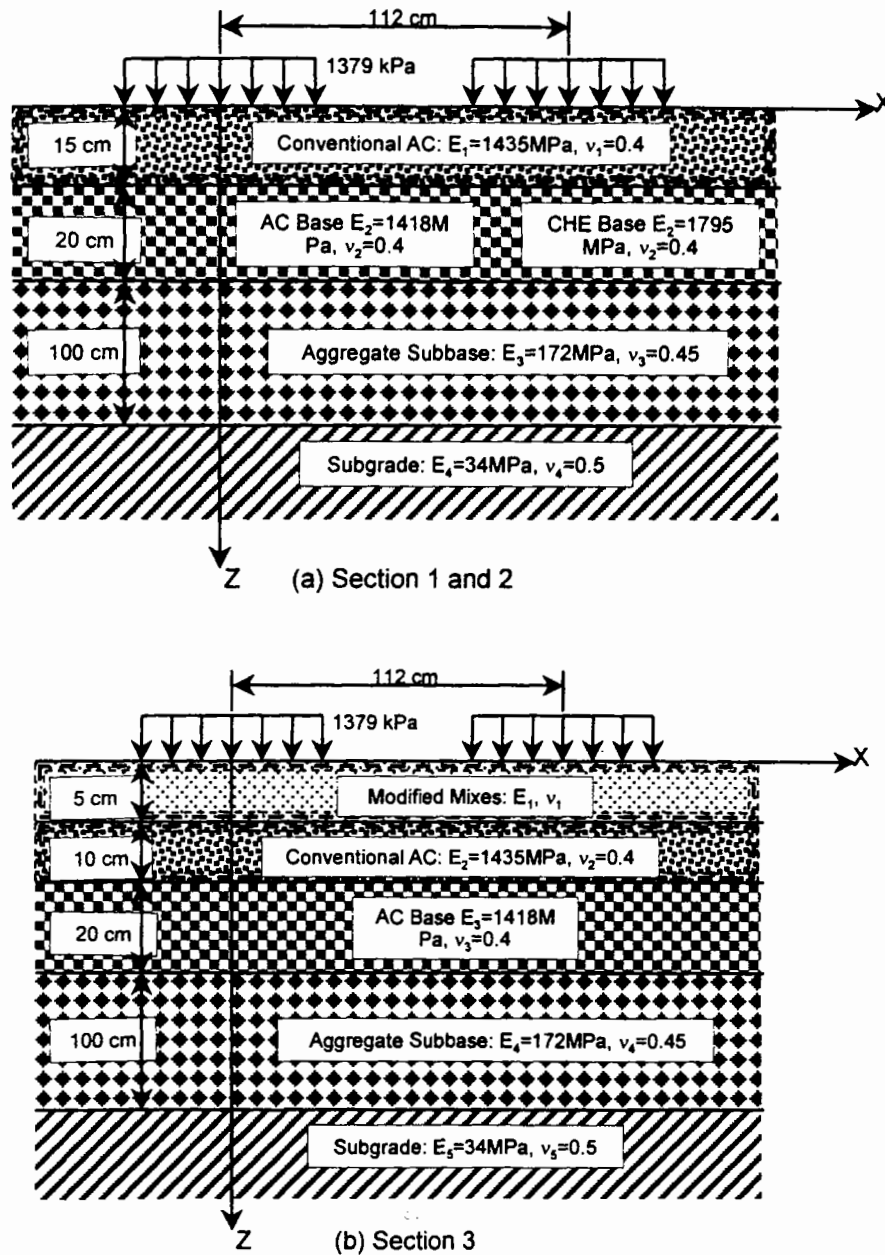


FIGURE 4 Pavement Sections Used in the Structural Analysis

pressure of 1379 kPa (200 psi). The distance between the centers of these two wheels is 112 cm.

For the structural analysis, the multi-layered elastic program ELSYM5 was used. Typical values of elastic modulus and Poisson's ratio for aggregate and cement

treated base layers and subgrade were assumed as shown in Figure 4. The values of elastic modulus for the five surface course materials and two base course materials were determined from the dynamic modulus curves in Figure 3 at a frequency of 5 Hz.

TABLE III Results of Fatigue Characterization ( $f = 5\text{ Hz}$ )

| Mixture             |                                     | S19                | GIL                | SBR                | SMA                | SBS                | B25     | CHE     |
|---------------------|-------------------------------------|--------------------|--------------------|--------------------|--------------------|--------------------|---------|---------|
| Coeff.<br>in Eq (6) | $\alpha_1$                          | 2.92               | 3.27               | 3.08               | 2.72               | 3.50               | 3.08    | 3.22    |
|                     | $ E^* $ , MPa                       | 1,435              | 1,665              | 1,364              | 1,420              | 1,369              | 1,418   | 1,795   |
|                     | $C_{11}$                            | 0.00196            | 0.00497            | 0.0152             | 0.00445            | 0.00370            | 0.00384 | 0.00118 |
|                     | $C_{12}$                            | 0.53               | 0.43               | 0.55               | 0.47               | 0.46               | 0.47    | 0.53    |
|                     | $p_1$                               | 2.372              | 2.864              | 2.386              | 2.442              | 2.890              | 2.611   | 2.513   |
| Fatigue<br>Pred.    | $S_{1f}$                            | 33,000             | 53,000             | 34,000             | 22,800             | 45,000             | 16,270  | 18,200  |
|                     | Tensile Strain ( $\times 10^{-4}$ ) | 3.90               | 3.61               | 4.042              | 3.952              | 4.03               | 5.509   | 4.992   |
|                     | $N_f$ , w/oRP                       | $2.22 \times 10^6$ | $1.92 \times 10^7$ | $3.26 \times 10^6$ | $5.53 \times 10^5$ | $2.22 \times 10^7$ | 67,860  | 201,920 |
|                     | Rank                                | 4                  | 2                  | 3                  | 5                  | 1                  | 2       | 1       |

For fatigue performance characterization, the maximum tensile strains developed at the bottoms of the conventional AC base layer (i.e., 35 cm below surface) and CHE layer under the dual wheel loads were analyzed by using ELSYM5 and are provided in Table III. The tensile strains at the bottom of the five surface course materials (i.e., 5 cm below surface) are also provided in this table.

#### Characterization of Fatigue Prediction Models

Controlled-strain uniaxial cyclic tests under four different strain amplitudes were performed to evaluate the fatigue performance of the five surface course and two base course materials. Using the experimental data obtained from the cyclic tests, fatigue lives ( $N_f$ ) were calculated. It is important to note that the fatigue life is defined as the number of cycles at which *pseudo stiffness* reaches 50% of the initial value. The choice of pseudo stiffness instead of stiffness is based on the fact that the stiffness reduction during fatigue cycles is due to both damage growth and viscoelasticity (i.e., the time dependence of the relaxation modulus). Working with the pseudo stiffness removes the relaxation effect in fatigue cycles from the overall reduction of stiffness, and therefore yields a failure criterion more directly related to cracking.

The average  $N_f$  values at different strain levels for the surface course and base course mixtures are plotted in Figures 5(a) and 5(b), respectively. Of the five surface course mixtures, it appears that SBS has the best and SMA has the worst fatigue performance. It is

more difficult to compare the base course mixtures, but it appears that at higher strain amplitudes, CHE has better fatigue performance than B25.

From regression analysis of this data, the phenomenological model coefficients in Equation (1) were determined for each mixture and are presented in Table IV. The model coefficient "b" describes the slope of the log-log relationship between strain amplitude and  $N_f$ . A greater value of "b" indicates that the fatigue performance of the mixture is more sensitive to strain amplitude. This means that a mixture such as SBR ( $b = -4.84$ ) will perform better than S19 ( $b = -6.054$ ) at high strain amplitudes but will approach and eventually fall below the performance of S19 as the strain amplitude becomes smaller. Careful examination of Figure 5(a) shows this occurring. Of course the coefficient "a" is needed for a complete description of the fatigue performance.

Another fatigue model employed in this study is the one proposed by Lee et al. (1999) as shown in Equation (8). The coefficients in the fatigue prediction model without rest periods in Equation (6) are presented in Table III. In the calculation of the model coefficients for each mixture, two sets of test data with different amplitudes were used to reduce the sample-to-sample variability in the analysis. The procedure for calculating these model coefficients is as follows:

- 1) Determine an average value of  $|E^*|$  for a mixture at the frequency of 5 Hz (Figure 3).
- 2) Determine an average value of "n" from the creep compliance data.

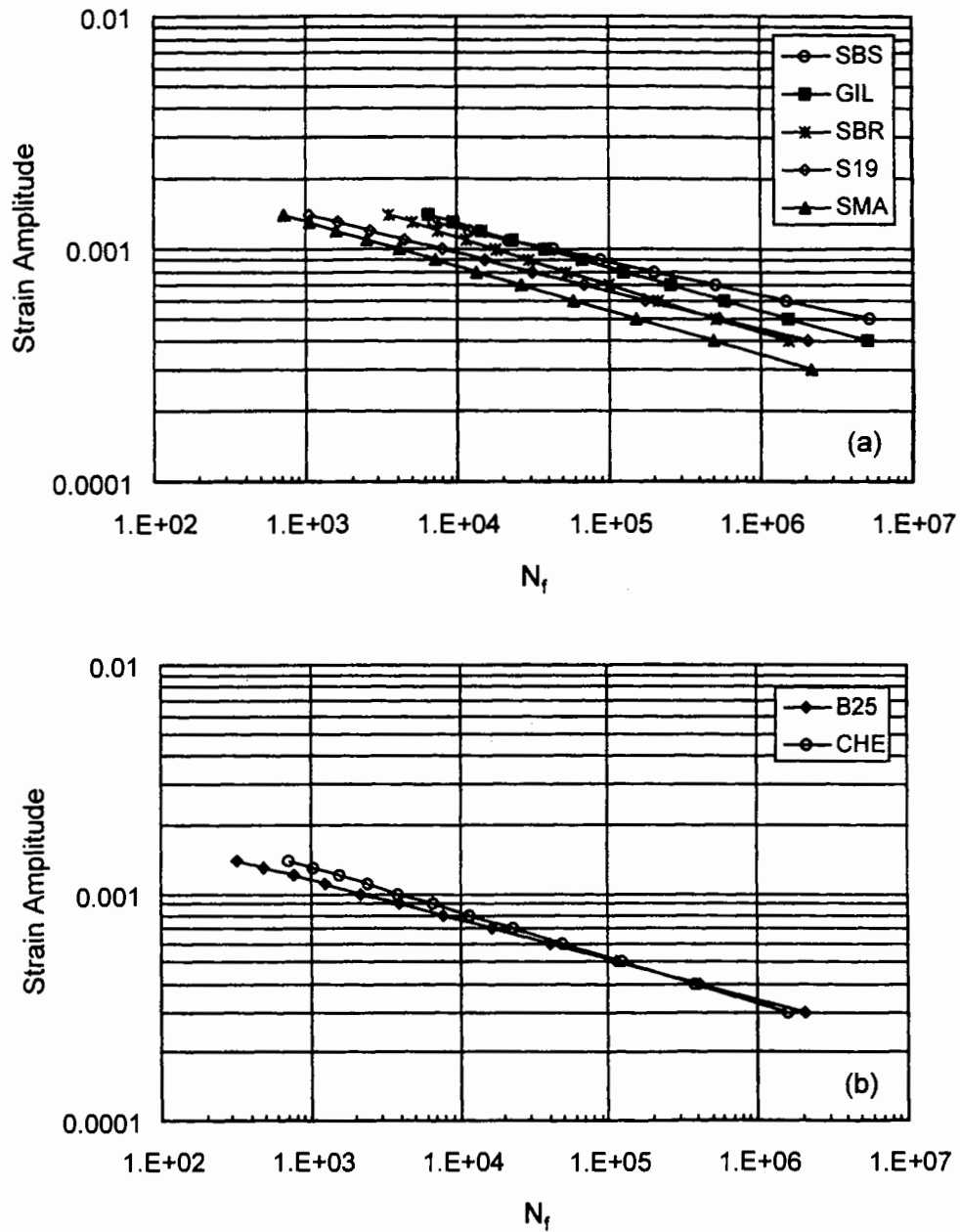


FIGURE 5 Fatigue Lives at Various Strain Amplitudes: (a) Surface Mixes; (b) Base Mixes (Data Points from the Regression Analysis)

3) Calculate the values of pseudo stiffness and  $S_1$  at each cycle collected during the test. Plot pseudo stiffness versus  $S_1$  using all available data and obtain the regression coefficients of the function  $C_1$  (i.e.,  $C_{11}$  and  $C_{12}$ ).

4) Calculate  $\alpha_1$  and  $p_1$ .

5) Back calculate an average value of  $S_{1f}$  from Equation (6) using measured  $N_f$  values and the coefficients obtained from steps 1)~4).

TABLE IV Comparison of Fatigue Model Coefficients

| Mixture                 | S19                   | GIL                   | SBR                   | SMA                   | SBS                   | B25                   | CHE                   |
|-------------------------|-----------------------|-----------------------|-----------------------|-----------------------|-----------------------|-----------------------|-----------------------|
| Eq (1) "a"              | $5.5 \times 10^{-15}$ | $3.8 \times 10^{-12}$ | $5.3 \times 10^{-11}$ | $9.6 \times 10^{-13}$ | $6.8 \times 10^{-17}$ | $1.7 \times 10^{-14}$ | $3.7 \times 10^{-12}$ |
| Eq (6) "A"              | $2.7 \times 10^{-14}$ | $5.9 \times 10^{-16}$ | $3.3 \times 10^{-18}$ | $1.7 \times 10^{-13}$ | $3.8 \times 10^{-17}$ | $4.1 \times 10^{-16}$ | $8.9 \times 10^{-17}$ |
| Eq (1) "b"              | -6.05                 | -5.33                 | -4.84                 | -5.21                 | -6.93                 | -5.70                 | -5.01                 |
| Eq (6) " $-2\alpha_1$ " | -5.84                 | -6.54                 | -6.16                 | -5.44                 | -7.0                  | -6.16                 | -6.44                 |

Using Equation (6) with the coefficients and tensile strain values shown in Table III, the values of  $N_f$  without rest periods are predicted and compared with the measured values in Figure 6. The data shown in this figure include the fatigue test data not used in the determination of the model coefficients. In general, a good agreement is found between the measured and the predicted fatigue lives, which demonstrates the validity of the fatigue prediction model in Equation (6). A similar verification result was observed in previous works (Lee et al. 1999) for two conventional asphalt mixtures. The verification result shown in Figure 6 implies that the fatigue model in Equation (6) can be applied to both conventional and modified asphalt mixtures.

Examining the predicted fatigue lives of the mixtures shown in Table III, SBS has the best and SMA the worst performance of the surface course mixtures and the CHE base course performs better than the B25 mixture. Examination of the base courses at a lower strain amplitude (0.0003) will show that the performance of B25 is better. It is noted from this table that the fatigue lives of the base course materials are much shorter than the fatigue lives of the surface materials. This implies that, for fatigue cracks originating at the bottom of the asphalt layer, the fatigue performance of the whole pavements is dominated by the fatigue life of base course material. That is, once the fatigue cracks begin to propagate from the bottom of the base layer, fatigue cracks may be observed on the surface of the pavement long before the fatigue life of the surface material is reached.

The weakening of the base course due to fatigue damage increases the tensile strain in the surface course, accelerating damage accumulation and hastening failure. However, for the fatigue cracks starting from the surface of the asphalt layer, the fatigue

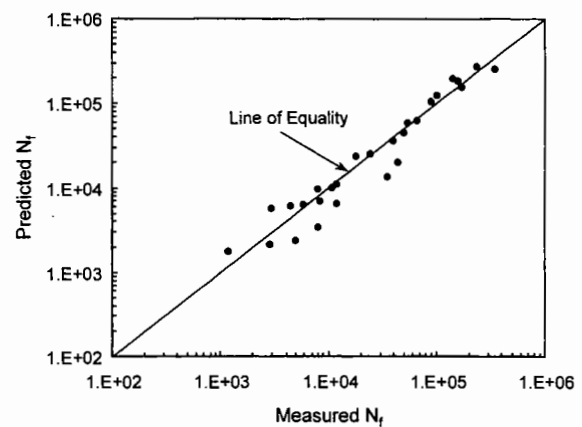


FIGURE 6 Validation Results of Fatigue Prediction Model in Equation (6)

resistance of the surface mixtures is still important. In this case, cracks may be developed due to a combination of complex fracture modes (e.g., crack opening mode, shearing mode, and tearing mode etc.). The uniaxial tension fatigue test may not be sufficient to consider all these mechanisms.

A comparison of the strain amplitude exponents in the phenomenological ("b" in Equation 1) and continuum damage ( $-2\alpha_1$  in Equation 6) models shows that the values are similar. However, one needs to be careful in comparing "a" from the phenomenological model with "A" in Equation (6). The coefficients that determine the value of "A" are all linear viscoelastic parameters, and are therefore strain independent. It must also be remembered that the phenomenological coefficients are determined from a direct regression of the strain amplitude versus  $N_f$  relationship. The continuum damage coefficients  $\alpha_1$ ,  $|E^*|$ , and  $p_1$  are determined from an independent creep test while  $C_{11}$ ,  $C_{12}$ , and  $S_{1f}$  are determined from the cyclic loading test.

The two models take completely different approaches to modeling the fatigue behavior, but result in similar values for the coefficients, as shown in Table IV. For the GIL, SBR, and CHE mixtures, the difference between “a” and “A” seems fairly large compared to the other mixtures. However, these mixtures also show a greater difference between “b” and  $-2\alpha_1$ , and it is the two coefficients together that describe the fatigue behavior of the mixture.

Combining the above observations with the discussion at the beginning of this section, one may begin to see how the material characteristics, properties, test conditions, and failure criterion affect the fatigue performance. The similarity between “b” and  $-2\alpha_1$  suggests that the slope of the creep compliance curve (from which  $\alpha_1$  is calculated) determines how sensitive the fatigue performance is to the applied strain amplitude. For instance, a lower value of “n” results in a lower value of  $-2\alpha_1$  and a mixture less sensitive to the strain level. This makes sense in respect to the creep compliance; that is, a flatter slope in a creep curve indicates that the material is more elastic and hence one would expect the response to be less sensitive to strain level.

It is difficult to examine the individual effects of the parameters in Equation (6) on the fatigue life because they are interdependent, meaning that changes in one parameter are associated with changes in another parameter. As an example, consider a mixture that is subject to aging. As the mixture ages, the viscoelastic properties change, affecting the damage evolution characteristics and ultimately, the  $S_{1f}$  value. Thus, accurate prediction of the fatigue life of this asphalt mixture would require not only loading conditions (e.g., tensile strain in the phenomenological model) and linear viscoelastic material properties (e.g., the slope of creep compliance versus time relationship in a logarithmic scale in more recent fatigue models), but also the determination of damage and microdamage healing characteristics.

It may not be possible to select a single parameter that governs the fatigue lives of asphalt mixtures because of the above reasons. However, it is still desirable to select one or two governing material properties to allow identification of better fatigue

resistant mixtures for design purposes. Thus, a careful investigation of the fatigue model in Equation (6) was performed. As can be seen in Equation (6), a higher value of  $S_{1f}$  and a lower value of  $|E^*|$  extend the fatigue life. Equation (4) shows that  $S_{1f}$  is proportional to the value of  $(\varepsilon_N^R)^{2\alpha_1/(1+\alpha_1)}$ . For the strain-controlled continuous cyclic loading,  $\varepsilon_N^R$  is equal to  $\varepsilon_0[E(t) + |E^*|]/2$  (Lee *et al.* 1999) and thus, a higher value of  $|E^*|$  is required to have a higher value of  $S_{1f}$ . This complicated interdependency implies that it may not be possible to identify a better fatigue resistant mixture only using  $|E^*|$ . It is clearly seen in Table IV that a significant relationship does not exist between the  $|E^*|$  values and the fatigue performance ranking.

Another important parameter affecting the fatigue life is  $\alpha_1$ . The  $\alpha_1$  value affects  $S_{1f}$ ,  $\varepsilon_0$ ,  $|E^*|$ ,  $C_{11}$ , and  $C_{12}$ . If the  $\alpha_1$  value increases,  $S_{1f}$  and  $\varepsilon_0^{-2\alpha_1}$  increase (increase in  $N_f$ ), but  $(C_{11}C_{12})^{-\alpha_1}$  and  $|E^*|^{-2\alpha_1}$  decrease (decrease in  $N_f$ ). It is seen from this observation that identifying the effects of  $\alpha_1$  on the  $N_f$  is very difficult without utilizing actual experiment data. It can be seen in Table III that  $\alpha_1$  is very well correlated with the fatigue performance ranking. That is, the higher the  $\alpha_1$  value (i.e., the lower the slope of creep compliance curve, n), the longer the fatigue life for surface and base mixtures, respectively.

It is noted in Table III that the SBR and B25, and GIL and CHE have similar  $\alpha_1$  values, but the fatigue lives of the surface versus base courses are significantly different. This is partially due to the fact that the levels of tensile strains between surface and base courses are quite different resulting in different fatigue lives. Therefore, it is unfair to compare fatigue lives of surface mixtures with those of base mixtures directly. However, if the base courses are evaluated at a strain level closer to those found in the surface courses ( $\varepsilon=0.0004$ ), the fatigue lives of B25 ( $3.5 \times 10^6$ ) and CHE ( $6.8 \times 10^6$ ) are similar to those of SBR ( $3.26 \times 10^6$ ) and GIL ( $1.92 \times 10^7$ ), respectively.

The value of  $S_{1f}$  also correlates well with the fatigue ranking because an increase in the  $\alpha_1$  results in an increase in the  $S_{1f}$ . The rank reversal of SBS and GIL mixtures is not unexpected due to the difference in  $|E^*|$  values and recalling that both  $|E^*|$  and  $\alpha_1$  affect

the value of  $S_{1f}$ . Other parameters in Table III,  $p_1$ ,  $C_{11}$ , and  $C_{12}$  do not correlate well with the fatigue performance ranking.

Several parameters ( $\alpha_1$  and  $S_{1f}$ ) appear to govern the fatigue behavior of these mixtures. However, it is not advisable to only consider these parameters when evaluating the fatigue behavior because even though they are highly influential, *all* of the parameters play a role in the fatigue performance. It is conceivable that a situation could occur where an unfavorable combination of other parameters could prevail over a ranking determined by just looking at one or two parameters. It must also be noted that these findings are a result of testing seven mixtures that have varying binder content and gradation, which will influence the fatigue performance as well.

### Effect of Rest Periods on Fatigue Life

To evaluate the effect of rest periods on fatigue life, controlled-strain cyclic loading tests with multiple rest periods were conducted at three different strain amplitudes for five surface course mixtures. In order to compare the healing potentials of the mixtures, the increase in pseudo stiffness (i.e.,  $C_2$ ) during multiple rest periods was calculated for the five surface course mixtures and is presented in Figure 7. The figure shows that the model is able to distinguish between the healing performance of the different mixtures.

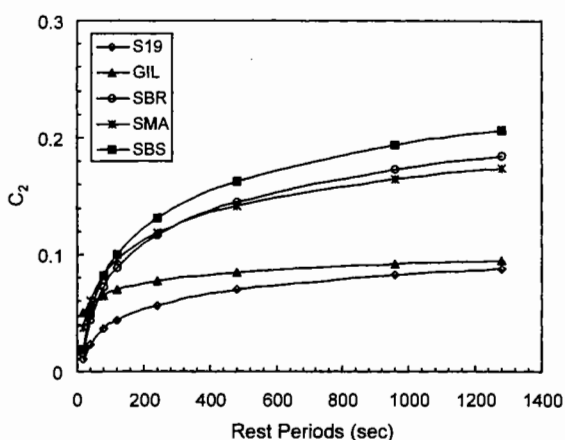


FIGURE 7 Increase in Pseudo Stiffness  $C_2$  During Rest Periods

The values of  $C_2$  in Figure 7 increase as the duration of rest increases. That is, the longer the rest period, the more the recovery of the damage. It is observed from this figure that the SBS shows the highest increase in pseudo stiffness during rest periods among five mixtures while the unmodified mixture S19 shows the lowest increase in pseudo stiffness. All four modified mixtures (GIL, SBR, SMA, and SBS) showed a better potential for healing than the S19 mixture.

The GIL mixture shows a large gain in  $C_2$  in the short term (quick healing), but levels out and longer rest periods have little beneficial effect. The SBS mixture, on the other hand, has a slower initial rate of healing, but continues to gain strength with time, indicating a better healing potential over time.

The amount of binder in the mixture will also affect the healing performance. Although the effect of binder content was not examined in this project, the relatively high binder content in the SMA mixture is probably the main reason for the good healing performance that was observed.

## CHARACTERIZATION OF RUTTING PERFORMANCE

### Test Results and Discussions

The rutting performance of a mixture can be affected by several factors such as aggregate gradation, angularity and texture of aggregate, asphalt content, and asphalt stiffness, etc. Of the mixtures tested during this study, S19, SBR, and GIL used the same gradation while SBS and SMA each used a different gradation. One type of asphalt binder was used in the mixtures but the stiffness of binder in each mixture was likely different due to the presence of modifier, and each mixture had its own binder content. For these reasons, it was not possible to evaluate the effect of modifiers on rutting performance in this study. However, it was possible to rank the mixtures in regards to their rutting performance, which was done by examining the vertical permanent deforma-

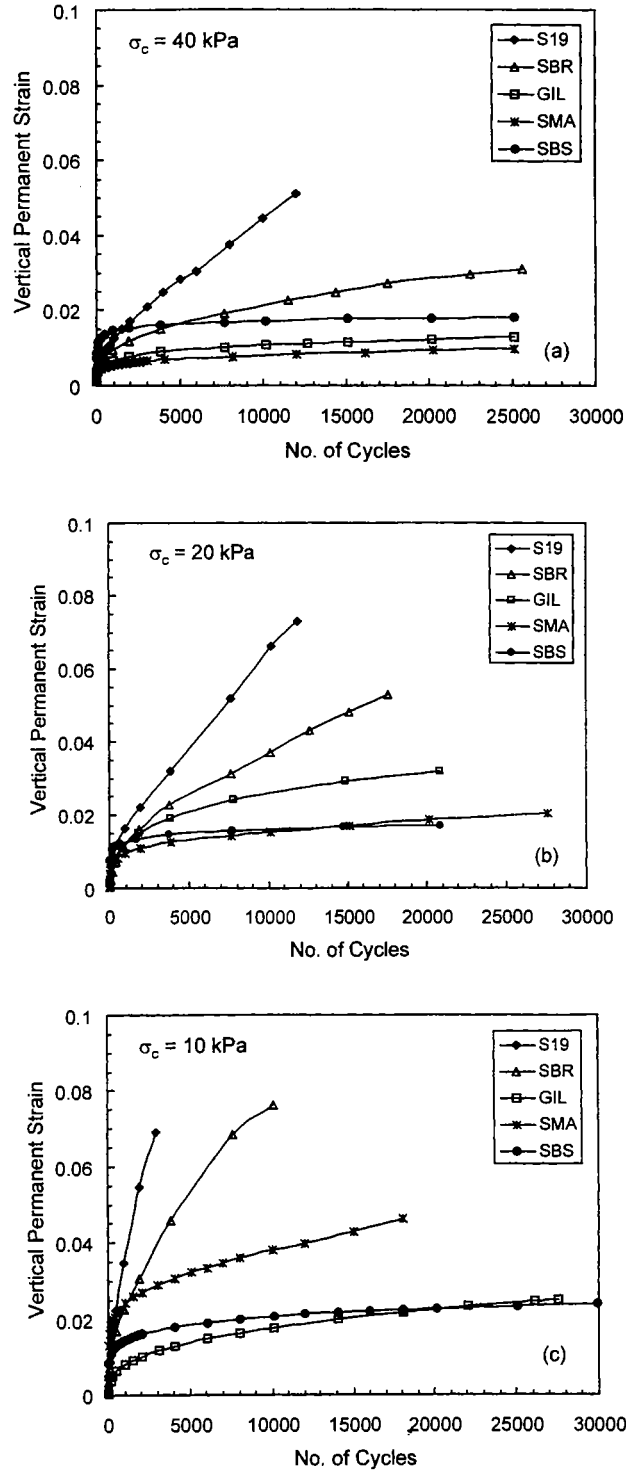


FIGURE 8 Increase in Permanent Strain at the Confining Pressures of: (a) 40 kPa; (b) 20 kPa; (c) 10 kPa

tion. The reader is reminded that the objective of this testing was a comparative analysis and therefore the reported values are not those that would be observed in the field under actual conditions.

Using the data obtained from triaxial tests, all the values of vertical permanent strain were calculated and are presented in Figures 8(a), 8(b), and 8(c) for 40, 20, and 10 kPa of confining pressures, respectively. It is clearly shown in these figures that the rutting performance of the modified mixtures including SBR, GIL, SMA, and SBS were better than the conventional S19 mixture. The SBS mixture shows the best rutting performance at confining pressures of 10 and 20 kPa while the SMA mixture shows the best performance at a confining pressure of 40 kPa. It is seen from these figures that more permanent strain occurs at lower confining pressures when the axial stress is constant. Also, it may be observed that the performance of SBS is less sensitive to confining pressure than SMA.

There are several reasons why the SBS may have showed good rutting performance. First could be the difference in grading; the SBS binder is graded (PG 76–22) and the ordinary binder (PG 64–16) is according to the Superpave binder specification. The difference in the PG grades clearly indicates that the SBS mixture will perform better at high temperatures and will be more resistant to rutting.

The second reason for the good performance of SBS could be the aggregate gradation. The aggregate gradation for the SBS mixture follows the recommendation in the Superpave mix design method (Asphalt Institute 1995) and passes below the restricted zone as shown in Figure 9(a). The S19 gradation passes above and through a portion of the Superpave restricted zone (Figure 9(b)). This could be another reason that the rutting performance of S19 mixture was the poorest, and the SBS among the best of the five surface course mixtures tested.

### Characterization of Permanent Deformation Model

The nature of Equation (9) requires that  $k_1$  and  $k_2$  be determined for each test. Therefore, the values of the

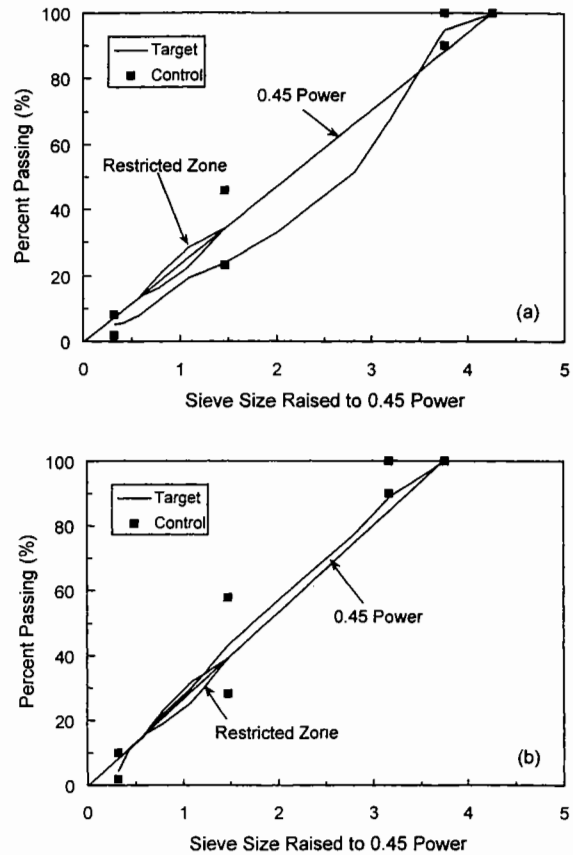


FIGURE 9 Comparison of Target Aggregate Gradations with Superpave Specification: (a) SBS Mixture; (b) S19 Mixture

coefficients vary with the applied stress level for a particular mixture. The permanent deformation model coefficients  $k_1$  and  $k_2$  in Equation (9) were first determined from a regression analysis of the triaxial test data shown in Figure 8. A relationship between the applied stress condition and the regression coefficients  $k_1$  and  $k_2$  was then developed.

First,  $k_1$  and  $k_2$  were separately regressed with respect to the  $p$  and  $q$  values of each stress condition. In general, the  $q$  values were better correlated with the coefficients  $k_1$  and  $k_2$ . The regression analysis conducted with respect to  $q$  resulted in an equation of the form:

$$k_1 = a_1 + a_2(q) \quad (10)$$

TABLE V Regression Coefficients for  $k_1$  and  $k_2$  in Equations (10) and (11)

| Mixtures   | Coefficients for $k_1$ |                        |       | Coefficients for $k_2$ |         |       |
|------------|------------------------|------------------------|-------|------------------------|---------|-------|
|            | $a_1$                  | $a_2$                  | $R^2$ | $b_1$                  | $b_2$   | $R^2$ |
| <b>S19</b> | 0.000446               | $2.5 \times 10^{-7}$   | –     | 0.03793                | 0.00219 | 91.1  |
| <b>GIL</b> | 0.00418                | $-1.23 \times 10^{-5}$ | 99.8  | -0.30941               | 0.00262 | 94.8  |
| <b>SBR</b> | 0.000398               | $1.50 \times 10^{-6}$  | –     | -0.0262                | 0.00205 | 66.4  |
| <b>SMA</b> | -0.0137                | $7.52 \times 10^{-5}$  | 68.5  | 0.15441                | 0.00018 | 83.3  |
| <b>SBS</b> | 0.0201                 | $-5.83 \times 10^{-5}$ | 99.8  | -0.15928               | 0.00117 | 85.2  |

where  $a_1$  and  $a_2$  are regression coefficients and are summarized in Table V. An average  $R^2$  value for all the mixtures was 89.4 percent. A similar relationship was developed for  $k_2$ :

$$k_2 = b_1 + b_2(q) \quad (11)$$

where  $b_1$  and  $b_2$  are regression coefficients and provided in Table V. An average  $R^2$  value for all the mixtures was 84.2 percent.

To estimate the permanent deformation in an asphalt layer of any thickness after the material has been characterized, the following layer-strain procedure (Barksdale 1972, Romain 1972) is suggested:

- 1) Depending on the thickness of the asphalt layer, it may be divided into several sublayers or remain as a single layer.
- 2) ELSYM5 is used to determine the stresses at the mid-depth of each sublayer.
- 3) The permanent deformation caused in each sublayer can be determined from Equations (9), (10), and (11) using the stress values determined in step 2).
- 4) The total permanent deformation in the asphalt concrete layer is then obtained by summing the contributions of all sublayers.

## CONCLUSIONS

In this study, rutting and fatigue performances of five surface and two base materials were characterized by performing uniaxial tension fatigue tests and triaxial compression tests, respectively. It was found that the simplified viscoelastic continuum damage mechanics-based fatigue prediction model proposed by Lee et

al. (1999) can be successfully applied to both conventional and modified asphalt mixtures.

The exponent of strain amplitude “b” in the phenomenological fatigue model in Equation (1) can be represented by the exponent of creep compliance curve “n” through “ $-2\alpha_1$ ” [i.e.,  $-2(1+1/n)$ ]. This implies that “n” is an indicator for the strain level sensitivity of the mixture. The parameter “n” is also an indicator for fatigue life at a *particular* strain level, meaning that “n” can be used to rank the performance of mixtures subject to the same, or similar strain level. A lower value of “n” indicates the mixture will have a longer fatigue life. Particular care must be taken however, because the strain level that a mixture will be subject to in the field is a function of both geometry (layer thickness) and the stiffness of the mixture itself. For this reason, using a single strain level to compare the fatigue performance of two mixtures with different stiffnesses placed in a similar pavement system is not recommended.

The damage parameter value at failure ( $S_{1f}$ ) was also strongly correlated with the fatigue life of the mixture. However, the material properties  $|E^*|$  and  $\alpha_1$  affect the damage parameter and must be considered when using  $S_{1f}$  to rank fatigue performance. Strictly based on the laboratory observations and considering the induced strain levels in the field, the SBS mixture has the best and the SMA mixture has the worst fatigue performance of the surface courses, while the CHE base course mixture performed better than B25.

The effect of rest periods on the fatigue lives of these mixtures was also evaluated in this study. Using the microdamage healing function,  $C_2$ , the model is able to distinguish healing performance among the

five surface course mixtures. The four modified mixtures display better healing potentials than the unmodified S19 mixture, with SBS showing the greatest increase in pseudo stiffness during rest periods.

Regarding the rutting performance of the mixtures, it was found that a linear relationship exists between the vertical permanent deformation and number of applied loads in a logarithmic scale and the vertical permanent deformation increases with an increase in  $q$  (shear stress invariant). The four modified mixtures performed better than the conventional S19 mixture, with the SBS mixture performing the best at the two lower confining pressures and the SMA mixture performing the best at high confining pressure. However, the differences in gradation and binder content among the different mixtures must be considered as they also affect rutting potential of a mixture.

Based on the comparison study of the performance of five surface mixtures, overall, the SBS mixture showed the best performance with regard to fatigue, healing, and rutting. It is also worth noting that all of the modified mixtures performed better than the single conventional mixture. Only the fatigue performance of the base course mixtures was investigated, and the CHE mixture displayed a greater fatigue resistance than the B25 mixture.

### Acknowledgements

This study is sponsored by Korea Research Foundation in the program year of 1998 and Korean Airport Construction Authority. The authors are grateful for their support.

### References

- Asphalt Institute (1995) Superpave Level 1 Mix Design. Superpave Series No. 2, Lexington, KY.
- Barksdale, R.D. (1972) Laboratory Evaluation of Rutting in Base Course Materials, *Proceedings, Third International Conference on the Structural Design of Asphalt Pavements*, Vol. 1, London.
- Brown, S.F. (1975) Improved Framework for Predicting Permanent Deformation in Asphalt Layers. *Transportation Research Record* 537.
- Brown, S.F. and Bell, C.A. (1977) The Prediction of Permanent Deformation in Asphalt Pavement. *Proceedings of the Forth International Conference on the Structural Design of Asphalt Pavements*. Vol. I, Ann Arbor, Michigan.
- Celard, B. (1977) ESSO Road Design Technology, *Proceedings of the Forth International Conference on the Structural Design of Asphalt Pavements*. Vol. I, Ann Arbor, Michigan.
- Dijk, w. van and Visser, W. (1977) The Energy Approach to Fatigue for Pavement Design. *Proceedings of the Association of Asphalt Paving Technologists*, Vol. 46, 1.
- Kim, N.S. (1994) Development of Performance Prediction Models for Asphalt Concrete Layers. Ph.D. Dissertation, Dept. of Civil Eng., North Carolina State University, Raleigh, NC.
- Kim, Y.R., Lee, H.J. and Little, D.N. (1997) Fatigue Characterization of Asphalt Concrete Using Viscoelasticity and Continuum Damage Theory. *Journal of the Association of Asphalt Paving Technologists*, Vol. 66, pp. 520–569.
- Lee, H.J. and Kim, Y.R. (1998a) A Uniaxial Viscoelastic Constitutive Model for Asphalt Concrete under Cyclic Loading. *Jr. of Eng. Mech.*, ASCE, Vol. 124, No. 1, 1998.
- Lee, H.J. and Kim, Y.R. (1998b) A Viscoelastic Continuum Damage Model of Asphalt Concrete with Healing. *Jr. of Engineering Mechanics*, ASCE, Vol. 124, No. 11, November 1998, pp. 1–9.
- Lee, H.J., Kim, Y.R., and Daniel, J.S. (1999) A Viscoelastic Continuum Damage Mechanics-Based Fatigue Prediction Model of Asphalt Concrete. *Jr. of Materials in Civil Engineering*, ASCE. (Accepted).
- Park, S.W., Kim, Y.R., and Schapery, R.A. (1996) A Viscoelastic Continuum Damage Model and Its Application to Uniaxial Behavior of Asphalt Concrete. *Mechanics of Materials*, 24, p 241–255.
- Romain, J.E. (1972) Rut Depth Prediction in Asphalt Pavements, *Proceedings, Third International Conference on the Structural Design of Asphalt Pavements*, Vol. 1, London.
- Schapery, R.A. (1984) Correspondence Principles and a Generalized J-integral for Large Deformation and Fracture Analysis of Viscoelastic Media. *Int. J. Fract.*, 25, pp. 195–223.
- Schapery, R.A. (1990) A Theory of Mechanical Behavior of Elastic Media with Growing Damage and Other Changes in Structure. *Jr. Mech. Phys. Solids*, 38, pp. 215–253.
- Sousa, J.B., Craus, J. and Monismith, C.L. (1990) Summary Report on Permanent Deformation in Asphalt Concrete. Institute of Transportation Studies, University of California at Berkeley.
- Wijeratne, A. and Sargious, M. (1987) Prediction of Rutting in Virgin and Recycled Asphalt Mixtures for Pavements Using Triaxial Tests. *Proceedings of the Association of Asphalt Paving Technologists*, Vol. 56.